Journal of Thermal Analysis and Calorimetry, Vol. 91 (2008) 3, 797–803

SYNTHESIS AND THERMAL DECOMPOSITION OF MIXED Gd–Nd OXALATES

A. Ubaldini[1,2], *C. Artini*[1*], *G. A. Costa*[1], *M. M. Carnasciali*[3] *and R. Masini*[4]

[1]INFM and DCCI, Via Dodecaneso 31, 16146 Genova, Italy
[2]NIMS, 1-1 Namiki, Tsukuba, Ibaraki 305-0044, Japan
[3]INSTM and DCCI, Via Dodecaneso 31, 16146 Genova, Italy
[4]CNR–IMEM, Via Dodecaneso 33, 16146 Genova, Italy

Several $(Gd_{1-x}Nd_x)_2[C_2O_4]_3 \cdot nH_2O$ samples ($0 \le x \le 1$) were prepared by a coprecipitation method: the precipitation is quantitative and all the samples are homogeneous in stoichiometry. XRD analyses have shown that a complete solid solution is formed over the whole range of compositions. The dried Gd rich oxalates have initially a low water content which gradually increases with the Nd content. All the oxalates decompose in O_2 around 700°C either into a single mixed oxide or in a mixture of oxides through several steps, which can be ascribed to the loss of water and CO_2.

Keywords: *oxalates, rare earths, TG/DTA analysis*

Introduction

Rare earth (RE) sesquioxides are interesting materials for their significant physical and chemical properties [1]. Actually, they are applied in many technological fields, such as catalysts for a large number of organic reactions [2–4], host materials for powerful lasers [5], improved phosphors [6] or precursors for superconductors [7]. Particularly, some superconducting cuprates, where two or three RE are simultaneously present, exhibit high critical temperature and current density [8].

Generally it is difficult to prepare homogeneous mixed RE oxides or even simply homogeneous mixtures of RE oxides following a classical solid state route, because of their high thermal stability and low diffusion coefficients [9, 10]. A well known and important tool for the preparation of mixed oxides is the thermal decomposition of previously synthesised organic or inorganic salts, like acetates, oxalates, hydroxides or carbonates [11–14]. These compounds decompose at relatively low temperature, usually below 700°C, into an oxide or a mixture of oxides. The decomposition path is often very complex and undergoes many intermediate steps [15–19], depending also on the utilized atmosphere. When it is possible to prepare a salt where the cations are homogeneously distributed, for example using the coprecipitation from a solution, the decomposition will lead to a mixed oxide or, at least, to a homogeneous mixture of oxides [16].

Rare earths oxalates have gained importance due to their various properties, mainly related to their ionic conduction or dielectric properties [20]. They are crystalline materials and are usually hydrated. The most known form at room temperature is the monoclinic decahydrated oxalate (space group $P2_{1/c}$) [20–22], even if the compound with six water molecules has been also reported [17, 23].

Many reports exist on the thermal decomposition of simple oxalates [12, 15, 19] but the mixed systems are not well known. This work focuses on the particularly interesting mixed oxalates of Gd and Nd, since the two pure oxides, when prepared at temperatures above 1000°C, have different structures at room temperature: Nd_2O_3 is hexagonal (space group P-3m1) and Gd_2O_3 is cubic (space group Ia3) [9, 10].

This work precedes a study of the pseudobinary phase diagram of the system Gd_2O_3/Nd_2O_3, where it is important to establish if the behaviour of the oxides can be ascribed only to their intrinsic characters rather than to the possible biphasicity of the starting oxalates.

In order to check the monophasicity of the system, several mixed $(Gd_{1-x}Nd_x)_2[C_2O_4]_3 \cdot nH_2O$ ($0 \le x \le 1$) were prepared using a standardized coprecipitation method. All the samples were characterised by X-ray diffraction (XRD), SEM-EDAX and micro-Raman analyses; their decomposition was analysed by TG and DTA analysis.

Experimental

All the $(Gd_{1-x}Nd_x)_2[C_2O_4]_3 \cdot nH_2O$ samples were prepared by a coprecipitation method, starting from

* Author for correspondence: cristinaartini@iol.it

1388–6150/$20.00

Akadémiai Kiadó, Budapest, Hungary
Springer, Dordrecht, The Netherlands

commercial Nd_2O_3 and Gd_2O_3 powders (Aldrich; 99.99%). They were weighed in order to have a value of x ranging from 0 to 1 with steps of 0.1. A solution was prepared from these oxides using a slight excess of HCl (13% mV^{-1}). In order to ensure a complete precipitation and to avoid any possible concentration gradient, the precipitation of a mixed oxalate was achieved by fast addition of a fresh prepared oxalic acid solution in large excess. The precipitate was filtered, washed with deionized water till no trace of the Cl^- anion was detected, and then dried in air at 80°C for 24 h. A little amount of each sample was dispersed in isopropanol and analysed by SEM-EDAX. The particle size distribution was determined from SEM images containing at least 400 particles, using a public domain plug-in software [24].

The structure of all the samples was investigated by X-ray powder diffraction using a Philips PW1830 diffractometer (CuK_α radiation) in the range $5<2\theta<90°$.

Gd rich samples were also put in direct contact with a small amount of deionized water for one day and then dried at room temperature (hereafter referred as 'aged samples').

All samples were further analyzed at room temperature by Raman spectroscopy using a Renishaw System 2000 Raman imaging microscope. The spectra were the result of 9 accumulations, each one lasting 10 s, collected using a 633 nm He–Ne laser; they were recorded on several points, with a magnification of 50x.

A Netzsch 408 TG/DTA unit was utilized for the decomposition studies performed on about 100 mg powdered samples. The thermal schedules of the measurements consisted of a heating step from room temperature up to 1100°C at 5°C min^{-1} in flowing oxygen (100 cm^3 min^{-1}), followed by an isothermal plateau for one hour and then by cooling down to room temperature. In order to observe possible differences in the reaction mechanisms, the thermal behaviour of $(Gd_{0.4}Nd_{0.6})_2[C_2O_4]_3{\cdot}nH_2O$ was studied under different atmospheres (stream of O_2 and air). Isothermal annealing experiments were performed at 190°C (6 h).

Results and discussion

Powders synthesis and characterisation

According to our experimental procedure, rare earth oxalates form following the reaction path:

$$(1-x)Gd_2O_{3(s)}+xNd_2O_{3(s)}+6HCl_{(aq)}\rightarrow \rightarrow 2(Gd_{1-x}Nd_x)Cl_{3(aq)}+3H_2O$$

$$2(Gd_{1-x}Nd_x)Cl_{3(aq)}+3H_2C_2O_4+nH_2O\rightarrow \rightarrow (Gd_{1-x}Nd_x)_2[C_2O_4]_3{\cdot}nH_2O_{(s)}+6HCl$$

Mixed oxalates begin to precipitate immediately after the addition of oxalic acid because of their high insolubility in water (for example K_{sp} for Nd oxalate is $3{\cdot}10^{-27}$ [25]), leading to the formation of small particles. SEM images of oxalates with x equal to 1, 0.5 and 0 are shown in Fig. 1a–d respectively.

The average composition of the precipitates is very close to the nominal one. For instance, EDAX analysis performed on many 5x5 μm^2 randomly selected areas yielded a Nd content of 28.3, 49.6, 80.5% for the oxalates corresponding to nominal x=0.3, 0.5, 0.8 respectively.

No great differences were detected from point to point, meaning that the precipitation was homogeneous and quantitative.

The aspect of the precipitates changes with x. For Nd oxalate the particles are not isolated crystals but rather aggregates of many thin crystals (some of these aggregates are shown, at higher magnification, in Fig. 1d).

These aggregates have an irregular shape, formed by small fused globes. Observed at higher magnification, these precipitated particles, composed of crystals with a nearly constant size, have either a cross-shaped or a 'pop-corn' like aspect. In any case, it is possible that the shape and the morphology of the particles might be modified by the high vacuum exploited during SEM analysis: the water is released in an abrupt way from the particles because of the low pressure.

These aggregates are, on the contrary, not very common for Gd oxalate, particularly the cross-shaped ones are absent. There are still many aggregates, but their shape is irregular and the number of isolated particles is higher.

On average an asymmetric distribution of the precipitate particle sizes is observed in both cases, peaked around 35 μm^2 for all the compositions. For x=1, due to the presence of the nearly spherical aggregates, a second value is observed at 110 μm^2.

The situation for x=0.5 seems to be intermediate, as the cross-shaped particles are practically absent and the aggregates show a more regular, almost spherical, shape.

The single crystals forming the aggregates are smaller and more uniform for high Nd contents. Generally they have a square or rectangular shape and, for $Nd_2[C_2O_4]_3{\cdot}nH_2O$, the average crystal size is about 2 μm x 2 μm, for $GdNd[C_2O_4]_3{\cdot}nH_2O$ it is about 4 μm x 4 μm and for $Gd_2[C_2O_4]_3{\cdot}nH_2O$ it is about 6 μm x 5 μm.

These results might indicate a different mechanism of formation for the oxalates of Nd and Gd. When the oxalic acid solution is added to the RE solution, even if it is vigorously stirred, the conditions for the formation of the precipitate are rapidly reached, as the

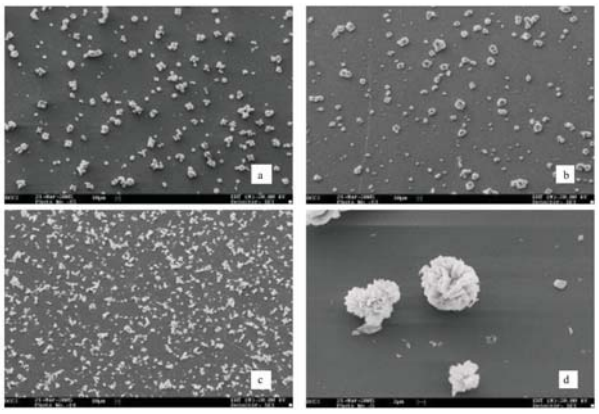

Fig. 1 SEM images of a – Nd oxalate (90x), b – ($Nd_{0.5}Gd_{0.5}$) oxalate (90x), c – Gd oxalate (90x) and d – Nd oxalate at higher magnification (800x)

concentration of $H_2C_2O_4$ and therefore of $C_2O_4^{2-}$ is locally high; thus several nuclei appear in small areas and many crystals quickly grow on them forming the aggregates. Their size increases and, as they become too heavy, they start to precipitate.

It seems that, dealing with Nd oxalate, the nucleation rate is high and likely greater than the crystal growth rate, so during the whole precipitation process a large number of nuclei form, leading to a wide distribution of aggregates sizes. It has been also reported that the solubility of the RE oxalates slightly increases with the RE atomic number [26]; thus, the nucleus critical radius for Nd oxalate could be smaller than for Gd oxalate. Small crystals can quickly appear in the solution and in very small areas: for this reason, they form immediately the aggregates.

For what concerns Gd oxalate, on the contrary, the nucleation rate seems to be lower compared to the previous case and some crystals can thus grow and reach larger dimensions. Furthermore, the shape is irregular because they form for random cohesion of isolated particles or smaller aggregates.

For the other compositions, the shape and the size of the aggregates change linearly as a function of the ratio Nd/Gd, meaning that the nucleation and the growth rate depend on *x*.

As shown by the X-ray analysis performed on the aged samples (Fig. 2), all the oxalates are crystalline; for clarity, only the diffraction patterns of the mixed oxalates with x =0, 0.5 and 1 are shown.

In any case the XRD patterns are very similar to those of other $RE_2[C_2O_4]_3 \cdot 10H_2O$ and all the peaks can be indexed assuming a monoclinic system with space group $P2_{1/c}$. The reported lattice constants both for Nd oxalate (*a*=11.192 Å, *b*=9. 612 Å, *c*=10.257 Å, β=114.42°) [22] and Gd oxalate (*a*=11.04 Å, *b*=9. 63 Å, *c*=10.09 Å, β=114.10°) [20] are close to those obtained (*a*=11.19 Å, *b*=9.66 Å, *c*=10.27 Å, β=114.25° for *x*=1 and *a*=11.02 Å, *b*=9.64 Å,

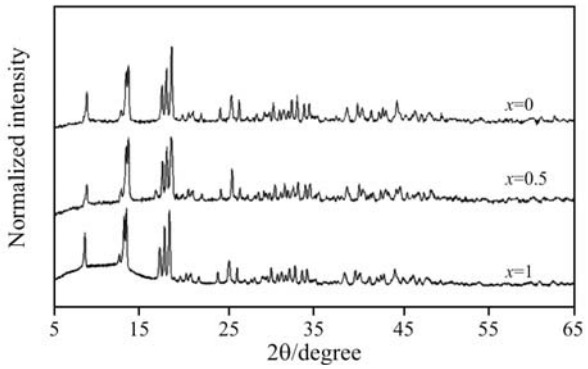

Fig. 2 Diffraction patterns of the aged oxalate with *x*=0, 0.5 and 1

c=10.04 Å, β=113.80° for *x*= 0). As shown in Fig. 3, a linear increase of all the cell parameters as a function of *x* is observed in agreement with the fact that Gd^{3+} is smaller than Nd^{3+}. The angle β is almost constant for both *x*=0 and *x*=1, so that a large variation as a function of the composition can not be expected.

Hence, we can state that a complete solid solution forms for all the *x* values and that the properties and the structures of the mixed oxides, formed by thermal decomposition of the oxalates, depend only on the composition and temperature and not on an eventual initial polyphasicity of the oxalates.

Some interesting observations can be drawn about the oven-dried samples, mainly for the Gd rich samples. Their XRD patterns, as shown in Fig. 4, display a different structure: new peaks are detected in the oven-dried samples. It is important to notice that the position of the peaks of the oven-dried samples depend on the composition: there is a systematic shift towards lower angles as *x* increases, in agreement with the different sizes of Gd^{3+} and Nd^{3+}.

According to the thermal analysis, discussed in the following section, RE oxalates can easily lose water and at higher temperature also CO_2. Depending on the synthesis procedure, after the drying stage the water content can be lower than the equilibrium value, and this water lack is expected to modify the crystalline structure of the samples as well.

A drying process at 105°C leads to an almost complete dehydration, while the same process at 190°C

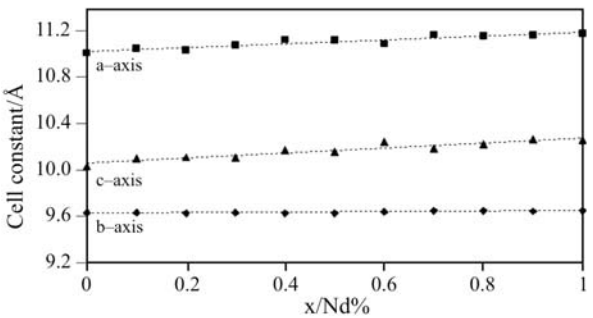

Fig. 3 Cell constants of the mixed Gd–Nd oxalates as a function of *x*

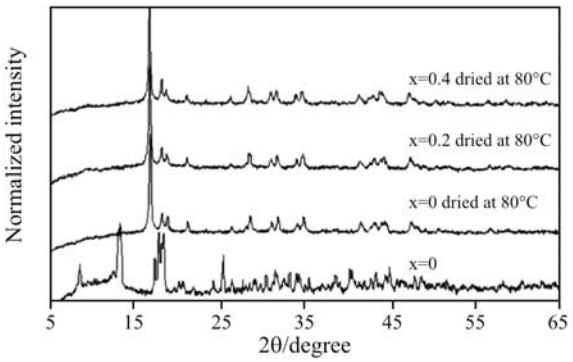

Fig. 4 Diffraction patterns of three Gd rich oxalates after the drying stage, compared to an aged sample

causes also the amorphization of the sample and the loss of some CO_2 molecules. A similar behaviour has been reported also for other oxalates. For instance, Hwu *et al*. [27] reported that $BaTiO(C_2O_4)_2{\cdot}4H_2O$ is crystalline and that the precipitate becomes amorphous as the drying temperature exceeds 100°C.

It has been observed that the hydration water can be fully recovered through an 'aging' process in a moist environment. This result highlights that the oxalates modify their structure and they can slowly reach the equilibrium content getting water from the atmosphere; this process is faster for Nd rich oxalates.

Thermal decomposition

A study of the thermal decomposition of rare earths mixed oxalates into their oxides is complex and uncommon in literature; only recently Ubaldini *et al*. [16] studied the thermal stability of the mixed Ce/Gd oxides.

The decomposition route of $(Gd_{0.2}Nd_{0.8})_2[C_2O_4]_3{\cdot}10H_2O$ is reported, as representative of the decomposition of all the Nd/Gd oxalates. Figure 5 shows DTA-TG analysis: many DTA signals and corresponding different TG steps can be noticed, meaning that many reactions occur during the decomposition. It is important to observe that, for temperatures above about 720°C, the sample mass is constant and no transformations occur, i.e. the

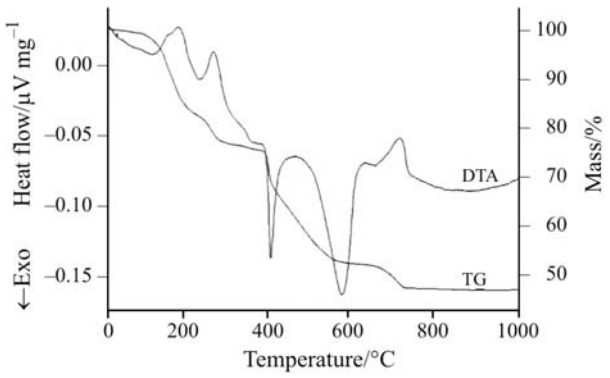

Fig. 5 TG-DTA analysis of $(Gd_{0.2}Nd_{0.8})_2[C_2O_4]_3$

initial system is completely converted into the oxide. Since it has been observed that lower heating rates result in a decrease of the transformation temperatures, we can conclude all the transformation temperatures depend on the heating rate. Furthermore, after a prolonged annealing (48 h) at 600°C, the oxalate was completely converted into the mixed oxide, suggesting that the equilibrium temperature can be close to this value, as confirmed for all the other rare earths oxalates [28].

The structure and the composition of the formed oxides depend on the decomposition temperature and on the ratio between Nd and Gd. For example, at 1200°C Gd_2O_3 is cubic, Nd_2O_3 is hexagonal and $NdGdO_3$, similarly to $LaGdO_3$ [29], is monoclinic. Moreover, solid solutions and biphasic regions exist, depending on the temperature. Detailed studies about the structure of the mixed oxides as a function of the temperature are in progress.

In the case of the decahydrated samples, the total mass loss is equal to the theoretical mass variation corresponding to the conversion of $(Gd_{1-x}Nd_x)_2[C_2O_4]_3{\cdot}10H_2O$ into $(Gd_{1-x}Nd_x)_2O_3$. In Table 1 the calculated and the experimental mass losses between 30 and 750°C for each value of x are shown: the percentage theoretical mass loss increases linearly as a function of x, as Nd is lighter than Gd, meaning that the decomposition is complete and effective.

For x=0.8, a slight loss of weakly bound water can be already observed from room temperature up to about 85°C. The water loss takes place in more steps: seven water molecules are lost at first and three more molecules afterwards. Two endothermic peaks are associated to these mass losses: the former with T onset at about 120°C, maximum at about 190°C and a shoulder at 160°C, the latter with T onset at about 235°C and a maximum at 270°C. Moreover, the

Table 1 Theoretical and experimental mass losses related to the transformation of $(Gd_{1-x}Nd_x)_2[C_2O_4]_3{\cdot}10H_2O$ into $(Gd_{1-x}Nd_x)_2O_3$ between 30 and 750°C

x	Theoretical mass loss/%	Experimental mass loss/%
0.0	52.22	51.94
0.1	52.40	52.36
0.2	52.58	52.65
0.3	52.76	52.63
0.4	52.94	52.90
0.5	53.13	53.19
0.6	53.32	52.35
0.7	53.50	53.50
0.8	53.69	53.62
0.9	53.88	53.98
1.0	54.07	54.28

former is composed of two partially overlapped signals that can be split in two different signals lowering the heating rate. For all the samples isothermal curves at 190°C show the total loss of water molecules associated with a slight CO_2 loss.

The mass variation of $(Nd_{0.8}Gd_{0.2})_2[C_2O_4]_3\cdot 10H_2O$ between 25 and 300°C is 24.4%, in agreement with the calculated value for a complete dehydration. Furthermore, the detected water loss signals are independent on the particular reaction atmosphere, while the subsequent exothermic signals are strongly affected: changing from O_2 to air, the signal at lower temperature is split, while the second one is shifted at higher temperatures.

For $Nd_2(C_2O_4)_3\cdot 10H_2O$, the experimental mass loss between 25°C and 200°C is 24.4%, i.e. very close to the calculated variation corresponding to the complete dehydration (24.6%). Associated to this step there is a large endothermic peak with maximum at about 150°C.

Considering DTA-TG analyses of $Gd_2[C_2O_4]_3\cdot 10H_2O$, in place of the two steps at low temperature related to the loss of water, five steps are detected, as reported in Table 2.

Table 2 Dehydration stages of $Gd_2(C_2O_4)_3\cdot 10H_2O$

ΔT/°C	Mass loss/%	Water molecules loss	Theoretical mass loss/%
25–75	2.3	1	2.4
25–100	4.3	2	4.8
25–125	>10	>4	9.4
25–200	18.5	8	18.7
25–300	23.5	10	23.7

Since a prolonged annealing near 100°C causes a partial dehydration of the product, this fact should be considered when dealing with samples dried in oven.

On the strength of the data, we can state that the dehydration path of Gd oxalate is consistent with the following:

$$Gd_2[C_2O_4]_3\cdot 10H_2O \rightarrow Gd_2[C_2O_4]_3\cdot 9H_2O + H_2O$$

$$Gd_2[C_2O_4]_3\cdot 9H_2O \rightarrow Gd_2[C_2O_4]_3\cdot 8H_2O + H_2O$$

$$Gd_2[C_2O_4]_3\cdot 8H_2O \rightarrow Gd_2[C_2O_4]_3\cdot 6H_2O + 2H_2O$$

$$Gd_2[C_2O_4]_3\cdot 6H_2O \rightarrow Gd_2[C_2O_4]_3\cdot 2H_2O + 4H_2O$$

$$Gd_2[C_2O_4]_3\cdot 2H_2O \rightarrow Gd_2[C_2O_4]_3 + 2H_2O$$

In the case of Gd oxalate the complete dehydration occurs in five steps, meaning that the molecules of water are not equivalent [16], in contrast to Nd oxalate, for which it is a two steps process: this different chemical equilibrium with water is due to their different cell parameters, that implies differently coordinated crystallization water.

The behavior of the other mixed oxalates is intermediate between the two previous cases. The average water coordination in the mixed oxalates depends on the ratio among the cations. In any case, the first molecules of water are weakly bound and can be easily removed from the oxalates. This can explain the different trend observed for the oven dried Gd rich oxalates: their total mass loss is smaller than the mass loss of the aged samples. Their behaviors are very similar above 300°C, namely where the decomposition of the anhydrous RE oxalate occurs. The n highest value for the oven-dried $(Gd_{0.5}Nd_{0.5})[C_2O_4]_3$ obtained in several preparations is 9, in agreement with the fact that this composition and Nd oxalate show the same XRD patterns.

For x=0.8 there is a mass loss which is over at about 580°C. The presence of two exothermic DTA peaks, the first one with an onset at 387 and maximum at 405°C and the second and greatest one, with an onset at 465 and maximum at 575°C, allows us to state that the decomposition of the anhydrous oxalate goes through the formation of the carbonate, $Gd_{0.4}Nd_{1.6}(CO_3)_3$, and through the formation of $Gd_{0.4}Nd_{1.6}O_{2+\delta}(CO_3)_{1-\delta}$, as reported for other RE oxalates [15, 17].

For x=1 the observed mass loss between 25 and 580°C is equal to 47.7%, corresponding to the theoretical mass variation related to the transformation of $Nd_2[C_2O_4]_3\cdot 10H_2O$ into $Nd_2O_2CO_3$, while the value due to the transformation of the oxalate decahydrated into $Nd_2(CO_3)_3$ is 35.8% and the experimental mass variation between room temperature and 420°C (corresponding to the offset temperature of the first exothermal peak and to a slope variation in the TG curve) is about 34%. We assumed that the initial stage of the decomposition of the anhydrous Nd oxalate is the formation of an amorphous Nd carbonate, as confirmed by our microRaman and XRD analyses. The formation of amorphous samples occurs between 190 and 550°C: above this temperature, the structures of the oxycarbonate at first and then of the oxide have been detected. Finally, between about 590 and 660°C the last mass loss is detected, corresponding to 5.1%, which is apparently associated to a weak and large endothermic DTA peak. In this step the decomposition of the oxycarbonate occurs.

It is particularly interesting to note that a prolonged annealing at constant temperature (550°C) results in a slight mass decrease with time and an endothermic DTA peak which develops at a critical mass loss. In these experimental conditions all the oxides considered [9, 30, 31] have a C-type structure that can change increasing the temperature.

Thus, in agreement with Nair *et al*. [28] it is possible to propose the decomposition of Nd decahydrated oxalate as follows

$$Nd_2[C_2O_4]_3\cdot 10H_2O \rightarrow Nd_2[C_2O_4]_3\cdot 8H_2O + 2H_2O$$
endothermic process - dehydration

$$Nd_2[C_2O_4]_3\cdot 8H_2O \rightarrow Nd_2[C_2O_4]_3 + 8\ H_2O$$
endothermic process - dehydration

$$Nd_2[C_2O_4]_3 + 3/2O_2 \rightarrow Nd_2(CO_3)_3 + 3CO_2$$
exothermic process - carbonate formation

$$Nd_2(CO_3)_3 \rightarrow Nd_2O_2CO_3 + 2CO_2$$
exothermic process - oxycarbonate formation

$$Nd_2OCO_3 \rightarrow Nd_2O_3 + CO_2$$
endothermic process - oxide formation

The last three stages can be recognized in all the mixed oxalates, meaning that the behavior of the anhydrous RE oxalates is similar, even if the temperatures of all the transformations increase with the Gd content. The thermal stability of the RE carbonate and oxycarbonate increases as a function of the molecular mass of the oxalate.

More significant differences in the oxalates dehydration path are observed, in agreement with [16–18, 23] who reported an 'inner core' composed by strongly bound water molecules. It must be noted, moreover, that the number of strongly bound water molecules in mixed oxalates depends on the Nd/Gd ratio.

A confirmation of the experimental results reported so far comes from Raman analysis performed on $Nd_2[C_2O_4]_3\cdot 10H_2O$ and $Gd_2[C_2O_4]_3\cdot 10H_2O$: in both cases, in the OH stretching region, there are some signals, due to crystallization water. Some differences exist, concerning the number of peaks and shoulders between Nd and Gd oxalate, confirming that the chemical bond with water is different in the two cases. In the mixed oxalates the positions and the forms of peaks in the OH region depend on the composition, showing a regular modification going from Nd to Gd oxalate.

The isolated oxalate ion has D2d symmetry and the group theory predicts 3A1+B1+2B2+3E Raman active modes [31]. For the various oxalates, the symmetry depends on the coordination with the metal [32].

Figure 6 shows the normalised Raman spectra of $(Gd_{1-x}Nd_x)_2[C_2O_4]_3$ (x=0.1, 0.3, 0.6, 0.8 and 1.0): they are consistent with the spectra of other metallic oxalates. The most intense peak is at about 1480 cm^{-1} and can be assigned to the n stretching mode of the CO group, being comparable with the reported wave number of the stretching mode of CO of other oxalates. For instance, it was reported that this band for potassium oxalate is at about 1496 cm^{-1}, for the calcium dihydrated

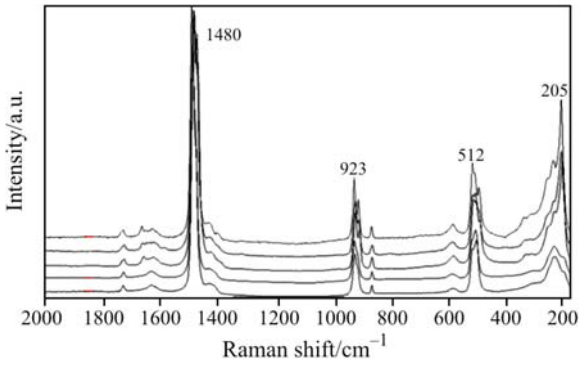

Fig. 6 Normalized Raman spectra of $(Gd_{1-x}Nd_x)_2[C_2O_4]_3$. From top to bottom x=0.1, 0.3, 0.6, 0.8 and 1.0

oxalate it is at about 1468 cm^{-1} and for the copper(II) oxalate it is at 1489 cm^{-1} [32, 33].

In all Raman spectra of the mixed oxalates the positions of the other peaks are similar, meaning that they slightly depend on the stoichiometry, even if they are a little different in the form: also in this case the modifications regularly follow the composition.

All the behaviours reported on Raman spectra are coherent with the results of the other techniques used in this work.

Conclusions

Several samples of Gd-Nd oxalates were prepared using a coprecipation method. The obtained mixed oxalates are decahydrated, but the Gd rich oxalates easily lose water during the first drying process.

The decomposition of the mixed oxalates is complex and it is complete below 700°C. $(Gd_{1-x}Nd_x)$ anhydrous oxalates decompose first in $(Gd_{1-x}Nd_x)_2(CO_3)_3$, then in $(Gd_{1-x}Nd_x)_2O_2CO_3$, and finally in the mixed oxides.

The different coordination of water molecules of Nd and Gd oxalate is evident in the Raman spectra: by this technique is also possible to compare the behaviour of the mixed oxalates.

XRD and DTA/TG analyses allowed to conclude that a solid solution forms for each x value. This is an important result for the preparation of Gd–Nd mixed oxides, because all the properties of the mixed oxides are intrinsic and depend only on their composition and thermal treatment temperature.

Such results allow to extend the same conclusions to other rare earth mixed oxides and, in particular, to perform the study of their pseudobinary phase diagrams.

Acknowledgements

The authors are very grateful to Dr. Giorgio Luciano for his helpful contribution.

References

1 G. A. M. Hussein, J. Anal. Appl. Pyrol. Sci., 37 (1996) 111.
2 A. G. Dedov and A. S. Loktev, Appl. Catal. A: Gen., 245 (2003) 209.
3 B. H. Davis and S. Brey, J. Catal., 25 (1972) 81.
4 R.-Q. Liu, Y.-H. Xie, J.-D. Wang, Z.-J. Li and B.-H. Wang, Solid State Ion., 177 (2006) 73.
5 R. Reisfeld and K. Jorgensen, Lasers and Excited States of Rare Earths, Springer, New York 1978.
6 E. Antic-Fidancev, J. Hölsa and M. Lastusaari, J. Alloys Compd., 341 (2002) 82.
7 P. Mele, C. Artini, R. Masini, G. A. Costa, A. Hu, N. Chikumoto and M. Murakami, Physica C, 391 (2003) 49.
8 A. Ubaldini, F. Giovannelli and I. Monot-Laffez, Physica, C, 383 (2003) 107.
9 R. G. Haire, L. Eyring, Handbook on the Physics and Chemistry of Rare Earths, K. A. Gschneidner Jr. and L. Eyring Eds, North-Holland Publishing Company, (1994) Vol. 18, p. 413.
10 G. Adachi and N. Imanaka, Chem. Rev., 98 (1998) 1479.
11 R. D. Purohit, S. Saha and A. K. Tyagi, Ceram. Int., 32 (2006) 143.
12 M. Popa and M. Kakihana, Solid State Ionics, 141–142 (2001) 265.
13 C. Peng, Y. Zhang, Z. W. Cheng, X. Cheng and J. Meng, J. Mater. Sci. Mater. Electr., 13 (2002) 757.
14 J.-G. Li, T. Ikegami, Y. Wang and T. Mori, J. Solid State Chem., 168 (2002) 52.
15 G. A. M. Hussein, M. H. Khedr and A. A. Farghali, Colloids Surf. A, 203 (2002) 137.
16 A. Ubaldini, C. Artini, G. A. Costa, M. M. Carnasciali and R. Masini, J. Therm. Anal. Cal., 84 (2006) 207.
17 B. A. A. Balboul, Thermochim. Acta, 351 (2000) 55.
18 D. Dollimore, Thermochim. Acta, 117 (1987) 331.
19 D. Zhan, C. Cong, K. Diakite, Y. Tao and K. Zhang, Thermochim. Acta, 430 (2005) 101.
20 A. Elizabeth, C. Joseph, I. Paul, M. A. Ittyachen, K. T. Mathew, A. Lonappan and J. Jacob, Mater. Sci. Eng. A, 391 (2005) 43.
21 E. Hansson, Acta Chem. Scand., 27 (1973) 2851.
22 W. Ollendorff and F. Weigel, Inorg. Nuclear Chem. Lett., 5 (1969) 263.
23 S. S. Moosath, J. Abraham and T. V. Swaminathan, Z. Anorg. Chem., 324 (1963) 103.
24 W. S. Rasband, Image, U. S. National Institutes of Health, Bethesda, Maryland, USA, http://rsb.info.nih.gov/ij/, 1997–2005.
25 R. Chi and Z. Xu, Metall. Mater. Trans. B, 30B (1999) 189.
26 Y. Minagawa and F. Yajima, Chem. Lett., 18 (1989) 2129.
27 J.-M. Hwu, W.-H. Yu, W.-C. Yang, Y.-W. Chen and Y.-Y. Chou, Mater. Res. Bull., 40 (2005) 1662.
28 K. G. Nair, V. V. Sreerajan and V. S. V. Nayar, Thermochim. Acta, 39 (1980) 253.
29 G. A. Tompsett, R. J. Phillips, N. N. Sammes and A. M. Cartner, Solid State Commun., 108 (1998) 655.
30 J. Tong and L. Eyring, J. Alloys Compd., 225 (1995) 139.
31 A. Ubaldini and M. M. Carnasciali, J. Alloys Compd., in press.
32 R. L. Frost, Anal. Chim. Acta, 517 (2004) 207.
33 H. G. M. Edwards and N. C. Russell, J. Mol. Struct., 443 (1998) 223.

Received: April 12, 2007
Accepted: September 18, 2007

DOI: 10.1007/s10973-007-8503-z